**Rui Liu**
Department of Mechanical Science and Engineering,
University of Illinois at Urbana-Champaign,
1206 W. Green Street,
Urbana, IL 61801
e-mail: ruiliu1@illinois.edu

**Surya P. Vanka**
Fellow ASME
Professor,
Department of Mechanical Science and Engineering,
University of Illinois at Urbana-Champaign,
1206 W. Green Street,
Urbana, IL 61801
e-mail: spvanka@illinois.edu

**Brian G. Thomas**
Professor,
Department of Mechanical Science and Engineering,
University of Illinois at Urbana-Champaign,
1206 W. Green Street,
Urbana, IL 61801
e-mail: bgthomas@illinois.edu

# Particle Transport and Deposition in a Turbulent Square Duct Flow With an Imposed Magnetic Field

*In this paper, we study particle transport and deposition in a turbulent square duct flow with an imposed magnetic field using direct numerical simulations (DNS) of the continuous flow and Lagrangian tracking of particles. The magnetic field and the velocity induce a current and the interaction of this current with the magnetic field generates a Lorentz force that brakes the flow and modifies the flow structure. A second-order accurate finite volume method is used to integrate the coupled Navier–Stokes and magnetohydrodynamic (MHD) equations and the solution procedure is implemented on a graphics processing unit (GPU). Magnetically nonconducting particles of different Stokes numbers are continuously injected at random locations in the inlet cross section of the duct and their rates of deposition on the duct walls are studied with and without a magnetic field. Because of the modified instantaneous turbulent flow structures as a result of the magnetic field, the deposition rates and patterns on the walls perpendicular to the magnetic field are lower than those on the walls parallel to the magnetic field.* [DOI: 10.1115/1.4027624]

## Introduction

Particle transport and deposition in turbulent flows are important in various industrial applications such as cyclone separators, dust collectors, spray combustion and transport, and entrapment of inclusion particles in continuous casting (CC) of steel. A large number of studies of particle motion and deposition in wall-bounded turbulent flows were performed by previous researchers through both numerical simulations [1–9] and experiments [10–12]. Among these, several studies of particle transport in turbulent flows in a square duct have been previously reported (e.g., Refs. [1–6]). Winkler et al. [1,2] performed large eddy simulations (LES) of particle transport in a square duct with different particle Stokes numbers and investigated the preferential concentration of the particles. They considered one-way, two-way, and four-way couplings between the continuous fluid and the discrete particle phase and simulated different particle volume fractions. They observed that the particle wall-normal deposition velocity increases with particle Stokes number, and mean secondary flows cause a wavy pattern of particle deposition velocities across the duct width. Winkler et al. [1] also studied preferential particle concentrations for different particle Stokes numbers. Their results show that particles accumulate in regions with high compressional strain and regions with low swirling strength. They demonstrated that vorticity is not always an accurate measure of preferential particle concentration, especially in the near-wall region where vorticity is dominated by shear.

Sharma and Phares [3,4] performed a DNS of turbulent flow in a square duct with Lagrangian particle tracking and studied the effects of particle inertia on particle dispersion and deposition on the duct sidewalls. They observed that higher-inertia particles tend to accumulate near the wall and mix more efficiently along the longitudinal direction, while particles with lower inertia are more likely to be sent to the near-wall region by the mean secondary flow and then drift back to the main stream, which is termed as particle resuspension. Yao et al. [5] also investigated particle resuspension in a turbulent square duct flow with a relatively high bulk Reynolds number of 250,000 using LES and a dynamic subgrid scale (SGS) model [13]. They found that for smaller particles (e.g., 5 $\mu$m particle diameter), particle resuspension is dominated by drag force due to the secondary flow, while for larger particles (e.g., 500 $\mu$m particle diameter), lift force cannot be neglected. They also evaluated the effect of gravity on particle resuspension and concluded that in their study gravity acts against particle resuspension [6].

Several experiments on the deposition rate of particles in wall-bounded flows have also been conducted for years [10–12]. Initial efforts were made by Friedlander and Johnstone [10], who studied transport and deposition rate of dust particles onto the walls of tubes. The re-entrainment of particles was reduced to a minimum by using adhesive material to keep deposited particles stuck on the walls. They also proposed a model of free-flight mechanism for particle depositions, based on experimental measurements and theoretical analysis. Liu and Agarwal [11] studied the turbulent deposition of aerosol particles in vertical pipe flows with different particle Stokes numbers (ranging from 0.21 to 771) for bulk Reynolds numbers of $10^4$ and $5 \times 10^4$. In their experiments, the maximum deposition rate occurred at particle Stokes number ($\tau_p^+$) equal to 30. They found that for particles with $\tau_p^+$ less than 10, the dimensionless particle deposition rate increases as the second power of particle response time and as fourth power of particle size. McCoy and Hanratty [12] examined the experimental data thoroughly from previous work and established the relationship between the dimensionless particle deposition rate and particle response time for different particle Stokes numbers. They also performed experimental studies of droplet deposition in a horizontal annular flow, the results of which reasonably fit their empirical correlation of the deposition rate with the particle response time.

In some industrial applications, electromagnetic devices such as MHD pumps and electromagnetic brakes (EMBr) are utilized to control the fluid dynamics of magnetically conducting fluids. It is found that when the flow is turbulent, the fluctuations are selectively damped by the magnetic field to the extent that the turbulence becomes two-dimensional. Quan et al. [14,15] conducted

Contributed by the Fluids Engineering Division of ASME for publication in the JOURNAL OF FLUIDS ENGINEERING. Manuscript received September 19, 2013; final manuscript received May 5, 2014; published online September 10, 2014. Assoc. Editor: Zhongquan Charlie Zheng.

  

LES simulations of the instantaneous liquid steel flow in the mold region of a continuous caster, in which inclusion particles were released from meniscus and upstream, and trajectories of particles were computed. Chaudhary et al. [16] performed LES simulations of liquid metal flow in a scaled model of a continuous casting mold and studied EMBr effects on the flow patterns. Chudhary et al. [17] also performed DNS simulations of the turbulent flow of a magnetic-conducting fluid in a square duct with imposed magnetic fields. The modification of the mean flow as well as near-wall turbulence by the imposed magnetic field is presented in this detailed study [17]. The modified turbulence field influences the mixing, particle transport, and heat transfer to the walls. Since the secondary flow significantly affects the pattern of particle deposition on square duct walls [1–6] and the applied magnetic field has a significant influence on the flow field, the particle dispersion and deposition in turn are also affected. Thus, study of particle behavior in turbulent flows with the effect of an imposed magnetic field is of importance both fundamentally and practically.

In this work, we study particle dispersion and deposition in turbulent flow in a square duct at $\mathrm{Re}_\tau = 360$ with a magnetic field using DNS of the continuous fluid and a Lagrangian particle-tracking scheme. A pressure-based finite volume approach implemented on a graphics processing unit (GPU) was used and particles with five different response times were considered. Particle dispersion, deposition locations, deposition velocities, and deposition rates for the different particle Stokes numbers were analyzed and compared with similar quantities without MHD effects. The deposition rates of particles in the non-MHD flow were confirmed to be in agreement with previous work [2], thus validating the particle module in the code. We observe that the particle deposition rate increases with particle response time (with particle Stokes number ranging from 0.1 to 15) for both MHD and non-MHD cases. However, deposition rates at duct walls parallel to the imposed magnetic field are found to be higher than that at walls perpendicular to the magnetic field.

## Numerical Formulation

Three sets of coupled equations are solved to describe the three different aspects of physics in this problem: the continuity and Navier–Stokes equations for the turbulent fluid flow, equations for the electric field, and equations for particle dynamics. For the continuous phase, the unsteady, incompressible three-dimensional continuity, and momentum equations given by

$$\nabla \cdot \mathbf{u}_f = 0 \tag{1}$$

$$\frac{\partial \mathbf{u}_f}{\partial t} + \nabla \cdot \left(\mathbf{u}_f \mathbf{u}_f\right) = -\nabla p + \frac{1}{\mathrm{Re}_\tau}\nabla^2 \mathbf{u}_f + \frac{\mathbf{f}}{\rho_f} \tag{2}$$

are solved. The source term $\mathbf{f}$ in Eq. (2) represents the Lorentz force, which is calculated by Eq. (3) with local current $\mathbf{J}$ and imposed magnetic field $\mathbf{B}_0$. The electric current in Eq. (3) is obtained from an electric potential and the instantaneous flow field, and the electric potential field is obtained by solving a Poisson equation given by Eq. (5).

$$\mathbf{f} = \mathbf{J} \times \mathbf{B}_0 \tag{3}$$

$$\mathbf{J} = \sigma\left(-\nabla\phi + \mathbf{u}_f \times \mathbf{B}_0\right) \tag{4}$$

$$\nabla^2\phi = \nabla \cdot \left(\mathbf{u}_f \times \mathbf{B}_0\right) \tag{5}$$

Calculations of particle dynamics are commonly based on the formulation by Maxey and Riley [18] for the forces acting on a rigid sphere in a nonuniform flow. These include the drag force, lift force, gravitational force, pressure and stress gradient forces, Basset history force, and added-mass force. Elghobashi and Truesdell [8] showed that for heavy particles (particles with high particle to fluid density ratio), only the drag force, lift force, and Basset history force are important for particle transport. However, they also pointed out that the Basset history force due to fluid acceleration is usually an order of magnitude smaller than the drag force. Thus, in the current study, only the drag force and the lift force are taken into consideration, and other forces are neglected. Particle trajectories are integrated from instantaneous particle velocities in the flow field via Eq. (6), and particle velocities are computed by solving the force balance equation shown in Eq. (7) below:

$$\frac{d\mathbf{x}_p}{dt} = \mathbf{u}_p \tag{6}$$

$$m_p \frac{d\mathbf{u}_p}{dt} = \mathbf{F}_D + \mathbf{F}_L \tag{7}$$

The two terms on the right-hand side of Eq. (7) are the drag force and the lift force. The drag force is calculated by Eq. (8), where the drag coefficient is calculated via a correlation [19] with particle Reynolds number given by Eq. (9).

$$\mathbf{F}_D = \frac{\pi}{8}\rho_f d_p^2 C_D \left|\mathbf{u}_f - \mathbf{u}_p\right|\left(\mathbf{u}_f - \mathbf{u}_p\right) \tag{8}$$

$$C_D = \frac{24}{\mathrm{Re}_p}\left(1 + 0.15\,\mathrm{Re}_p^{0.687}\right), \quad \mathrm{Re}_p = \frac{\rho_f d_p \left|\mathbf{u}_f - \mathbf{u}_p\right|}{\mu_f} \tag{9}$$

The lift force is calculated by the relation proposed by Saffman [20] given by Eq. (10)

$$\mathbf{F}_L = 1.61 d_p^2 \left(\rho_f \mu_f\right)^{1/2} \left|\nabla \times \mathbf{u}_f\right|^{-1/2} \left[\left(\mathbf{u}_f - \mathbf{u}_p\right) \times \left(\nabla \times \mathbf{u}_f\right)\right] \tag{10}$$

The particle response time is defined in Eq. (11), which reflects the time needed for a particle to accelerate from a stationary state to about 63% of surrounding fluid velocity.

$$\tau_p = \frac{\rho_p d_p^2}{18\mu_f} \tag{11}$$

The particle Stokes number is defined as the dimensionless particle response time in wall units, as shown in Eq. (12) below:

$$\tau_p^+ = \frac{\rho_f u_\tau^2 \tau_p}{\mu_f} \tag{12}$$

The computational domain considered here has dimensions $L_x \times L_y \times L_z = 8 \times 1 \times 1$, in the streamwise ($x$-axis), parallel ($y$-axis), and transverse ($z$-axis) directions, respectively. The imposed magnetic field is placed along the $z$-axis, pointing from the bottom wall to the top wall of the square duct, as shown in Fig. 1.

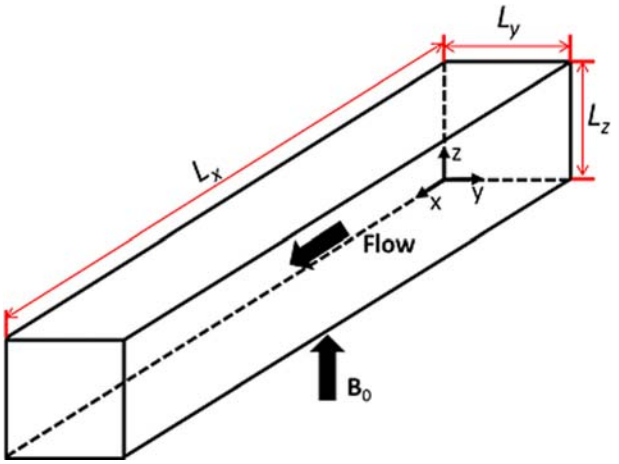


**Fig. 1 Schematic of computational domain**

The fluid flow equations are solved with a periodic boundary condition in the streamwise direction and no-slip conditions on the four sidewalls. For the electric potential, insulating duct walls are assumed and Neumann boundary conditions are prescribed. Thus, at walls $y=0$ and $y=1$ (parallel to magnetic field)

$$u_x = 0, \quad u_y = 0, \quad u_z = 0, \quad \frac{\partial \phi}{\partial y} = 0 \tag{13}$$

and at walls $z=0$ and $z=1$ (perpendicular to magnetic field)

$$u_x = 0, \quad u_y = 0, \quad u_z = 0, \quad \frac{\partial \phi}{\partial z} = 0 \tag{14}$$

In previous studies [1–6], streamwise periodic boundary conditions on particle positions were commonly used to study particle transport in the square duct. This treatment of particle boundary condition has two issues. First, because of periodic recycling, all particles that were originally injected in the domain will eventually deposit on the sidewalls. Thus, the particle volume fraction in the domain keeps decreasing with time, as happens in a very long duct. However, for parametric studies, it is desirable to keep a nearly constant particle volume fraction. Second, in studying particle dispersion along the longitudinal direction of the square duct, particles distributed at different locations initially in the domain will travel at different streamwise velocities, and particles near the walls will have much lower streamwise velocities compared with particles in the core region. The number of "duct lengths" has to be counted for each particle in order to study particle dispersion and deposition along the longitudinal direction.

In this work, we therefore followed a different practice of continuously injecting particles at the inlet ($x=0$) equal to the sum of particles depositing on the walls and exiting the domain. The initial locations of particles at the domain inlet are randomly distributed, and the initial particle velocities are set to be equal to the local fluid velocity. When a particle travels out of the computational domain, it is not recycled back to the domain (as in the case of periodic boundary condition) but leaves the domain forever. At sidewalls particle boundary conditions are set as completely absorbing. Once the distance between the center of particle and the wall is less than one particle radius, the particle is considered to be deposited on the duct wall.

The coupled equations of fluid flow and MHD are discretized with $80 \times 80 \times 512$ cells on a stretched Cartesian mesh with a stretching ratio of 1.01 from duct walls toward duct centerlines. The convection and diffusion terms in the momentum equations are discretized using a second-order Adams–Bashforth scheme and a fractional step method is used to project the pressure field to a divergence-free space. The resultant pressure Poisson's equation is solved using a geometric multigrid technique with red-black successive over-relaxation (SOR) scheme. The equation for the electric potential is solved with the same algorithm [16,17].

Particle positions are obtained using the trapezoidal rule, and the particle velocity is integrated using a fourth-order Runge–Kutta method. Fluid velocities at particle locations are interpolated using the 3D Lagrange cubic interpolation function from a $3 \times 3 \times 3$ cell block surrounding the particle, as shown in Eq. (15), and the Lagrange multipliers are defined in Eq. (16).

$$\varphi_p = \sum_{n=1}^{27} L_x^{ni} L_y^{nj} L_z^{nk} \varphi_n \tag{15}$$

$$L_x^{ni} = \prod_{i=1, ni \neq i}^{3} \frac{(x_p - x_i)}{(x_{ni} - x_i)}, L_y^{nj} = \prod_{j=1, nj \neq j}^{3} \frac{(y_p - y_j)}{(y_{nj} - y_j)},$$
$$L_z^{nk} = \prod_{k=1, nk \neq k}^{3} \frac{(z_p - z_k)}{(z_{nk} - z_k)} \tag{16}$$

The discretized set of flow equations, electrical potential equation, and the particle transport equations are together solved on a Tesla C2075 GPU chip. Each computational cell is mapped to a GPU thread, and the flow and MHD equations (where applicable) were solved in time without the particle phase. The details of solving the pressure Poisson's equation (PPE) and electric potential equation using a red-black Gauss–Seidel iterative solver with geometric multigrid technique on GPU were previously addressed by Shinn [21] and Chaudhary et al. [17] For particle simulations, each particle is assigned to an individual GPU thread and computational cells containing the particles are searched based on the updated particle positions from the previous time step. The fluid velocities are interpolated onto the particle locations following Eqs. (13) and (14), and slip velocities and drag and lift forces are calculated in parallel for all the particles. The velocity and trajectories of the particles are updated in parallel following Eqs. (6) and (7).

The flow Reynolds number based on the friction velocity ($\mathrm{Re}_\tau$) was 360 and in the MHD simulation, the Hartmann number was 21.2, for which the flow was still turbulent and not fully laminarized. The corresponding bulk Reynolds number was around 5000, and periodic boundary conditions were used in the streamwise direction. An $80 \times 80$ nonuniform finite volume grid in the cross section and 512 uniform finite volumes in the streamwise direction with $\Delta x^+ = 5.6$ were used. In order to demonstrate the adequacy of the mesh resolution, mean streamwise velocity profiles along both horizontal and vertical duct bisectors are plotted in Fig. 2 and compared with those of Chaudhary et al. [17] for a mesh of $128 \times 128 \times 512$ cells and same flow parameters ($\mathrm{Re}_\tau = 360$, $\mathrm{Ha} = 21.2$). As shown in Fig. 2, very good agreement has been obtained between the two sets of results, which suggests that the results are grid independent. It can be seen that mean velocity profile along the vertical bisector of the square duct is less flattened compared with that along the horizontal duct bisector as a result of turbulence suppression close to the top and bottom duct walls, which are perpendicular to the imposed magnetic field.

To initiate the computations, a laminar velocity profile with imposed perturbations for the first 1500 time steps was prescribed. A stationary state of the continuous flow was first obtained before particles were injected at the inlet plane. A total of 3,000,000 time steps were computed to get good stationarity of the flow, which was assessed by the attainment of a time invariant time-averaged velocity field. Table 1 gives the details of the particles released identically in the MHD and non-MHD simulations. Particle dispersion and deposition are a function of the nondimensional response time (particle Stokes number), which ranged between 0.1 and 15, and was modified by varying the particle diameter. The fluid density was set to unity, and its dynamic viscosity was set to 0.00264. The particle to fluid density ratio was set to a value of 1000. Larger particles respond less to the instantaneous flows and concentrate differently from the smaller particles. For dilute particle loadings, the one way coupling is a valid assumption. Although, Elghobashi [8] recommends a criterion of $10^{-6}$ below which the one-way coupling is definitely applicable, this criterion makes the particle loading very dilute to get a large enough sampling size. Winkler et al. [2] performed simulations of particle-laden flow in a square duct (without MHD effects) with a similar computational algorithm as in the current work and found that the particle deposition patterns with one-way coupling were in close agreement with those of a four-way coupling calculation for particle volume fractions around $10^{-4}$ and particle Stokes numbers between 0.1 and 30. Based on this observation, we have currently used a maximum volume fraction of the particle phase to be $10^{-4}$.

## Results and Discussion

**Continuous Flow Fields.** In a turbulent flow, particle transport is significantly more complex than in a laminar steady flow. Because of the turbulent fluctuating flow and the vortical

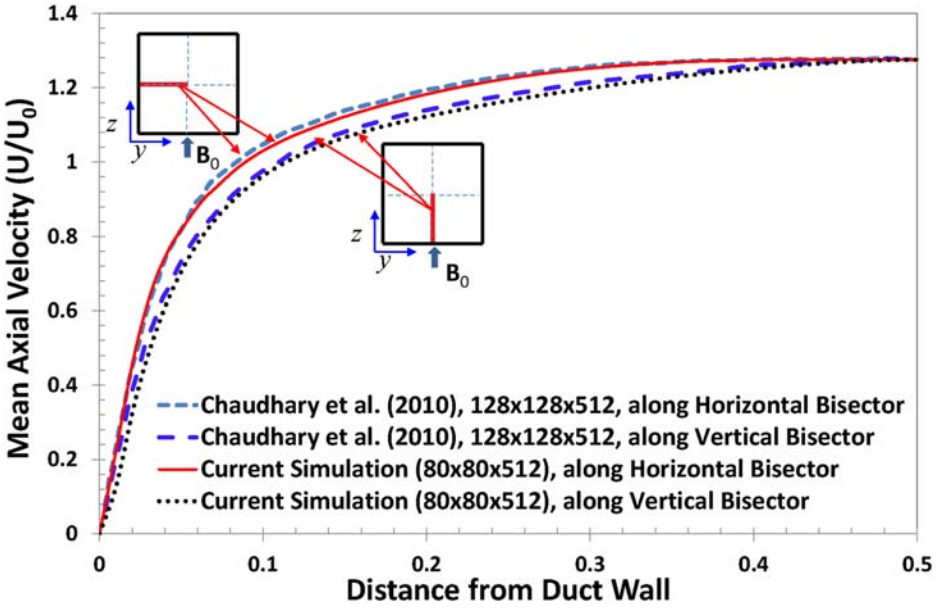


**Fig. 2 Velocity profiles along horizontal and vertical bisectors in MHD duct flow**

**Table 1 Particle properties used in the simulation**

| Particle stokes number $\tau_p^+$ | Particle diameter $d_p$ | Response time $\tau_p$ | Particle volume fraction $\phi_v$ |
|---|---|---|---|
| 0.1 | 0.000118 | 0.000293 | $5.356 \times 10^{-8}$ |
| 1 | 0.000373 | 0.00293 | $1.694 \times 10^{-6}$ |
| 5 | 0.000833 | 0.0146 | $1.894 \times 10^{-5}$ |
| 10 | 0.00118 | 0.0293 | $5.356 \times 10^{-5}$ |
| 15 | 0.00144 | 0.0439 | $9.840 \times 10^{-5}$ |

structures, at any instant in the simulation, the local velocities provide the instantaneous drag and lift forces based on positional velocity vector and the particle parameters. Hence, the generation of the continuous flow field is quite important to describing particle dynamics in an accurate way. In our study, we have first generated a statistically stationary flow by integrating the discrete equations until the ensemble-averaged flow field reached a stationary state. Particles of desired size were then released while the continuous flow equations were also being integrated. Since the instantaneous and time-averaged flow fields for a MHD duct flow are significantly different from those of a non-MHD case, it is expected that the dispersion and deposition characteristics will be quite different for the two cases and also will depend in a complex way on the particle Stokes number.

For a given continuous flow, the dispersion and deposition characteristics will also depend on the manner by which the particles are injected in the duct. In several previous studies (such as Refs. [1–6]), the particle positions were "recycled" from the duct exit to the entrance of the periodic duct, thus simulating a long fully developed duct flow. However, in such a case, the particle statistics will depend on the length of the integration time (equivalent to duct length). Also, only an average behavior over the duct length and integration time is obtained. Instead, in the present study, we inject the particles continuously at the inlet at randomly selected cross-sectional positions. The number of particles injected at any time equals the sum of number deposited and the number of particles exiting the outlet so that the total number of particles in the computational domain remains the same. Thus, the statistics of the deposition correspond to a fixed length of duct with averaging only in time. The particle deposition will therefore be a function of duct axial length and fully reflects the physics of the particle deposition.

Figures 3(*a*) and 3(*b*) show representative instantaneous velocity fields at cross-stream planes for the non-MHD and MHD cases, respectively. The contours correspond to streamwise velocity, while the vectors indicate the cross-stream secondary flow. The instantaneous secondary velocities are typically 8–10% of the local instantaneous streamwise velocities but when averaged in time reduce to much smaller time-averaged values. As a result, modeling the particle dynamics using Reynolds-averaged turbulent fields is quite difficult since the extraction of the instantaneous flow "backward" is not possible. DNS provides the time instantaneous flow fields, although being limited to low Reynolds numbers.

It can be seen that the MHD and non-MHD instantaneous flow fields are considerably different. This is because of the additional $(\mathbf{J} \times \mathbf{B}_0)$ force acting in the $x$- and $y$-directions. The additional force in the streamwise direction suppresses streamwise turbulence intensity while the $x$-direction force acts to modify the cross-stream turbulence. Since Chaudhary et al. [17] have already reported the rms statistics as well as the turbulent kinetic energy budgets, we limit our discussion to the particle dynamics only and provide the flow fields for completeness. Further, due to the assumption of the one-way coupling, the continuous flow field remains the same (statistically) as the no-particle case previously reported by Chaudhary et al. [17].

Figures 4(*a*) and 4(*b*) show the ensemble–averaged secondary flows and the contours of streamwise velocity. For the non-MHD case, the flow is symmetric about one-eighth of the duct, taking into account proper reflections. However, with MHD, there is only symmetry about one-fourth of the duct with reflection. The mean secondary flow eddies in the MHD case are stronger at the top and bottom walls (perpendicular to the magnetic field) and smaller toward the center of the walls and the duct corners. The mean streamwise velocity distribution is also modified by this drifting velocity, shrinking along the magnetic field direction. Eddies along the sidewalls parallel to the magnetic field are weakened but get closer to corners. This modification of mean secondary flow pattern will significantly change the pattern of particle deposition. While the mean flow field does not adequately characterize the particle dynamics, it is the one that is often predicted in engineering simulations and supplemented with models for stochastic dispersion. However, such predictions can be grossly in error because of the complex turbulent fields.

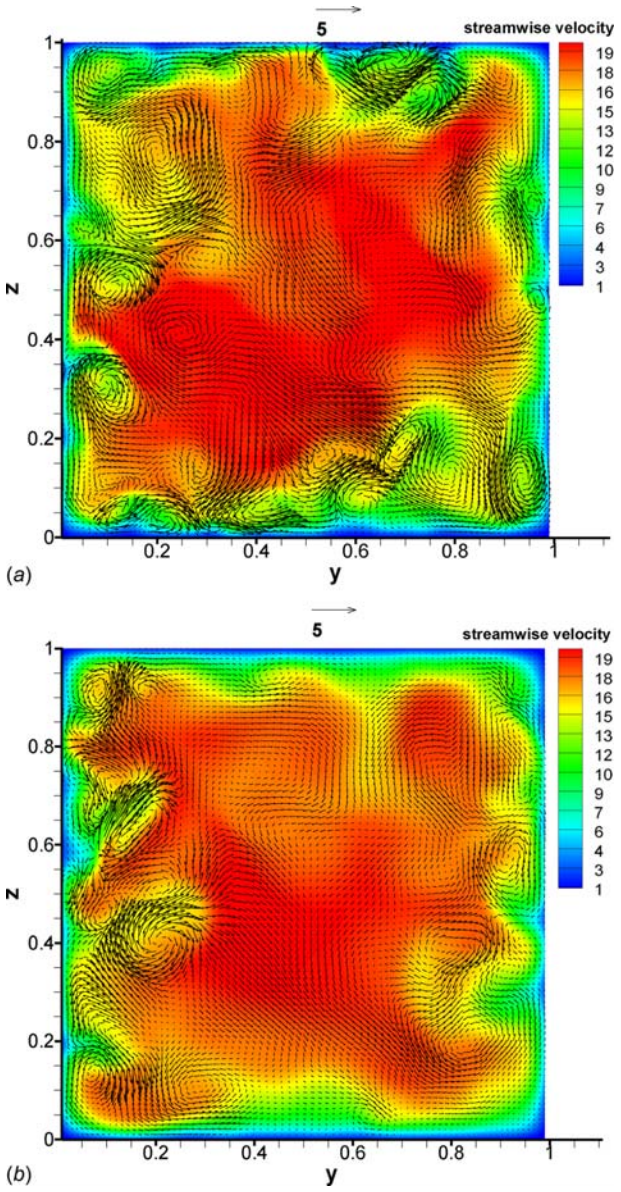


**Fig. 3 Instantaneous velocity field in a cross-sectional plane (*a*) non-MHD case and (*b*) MHD case**

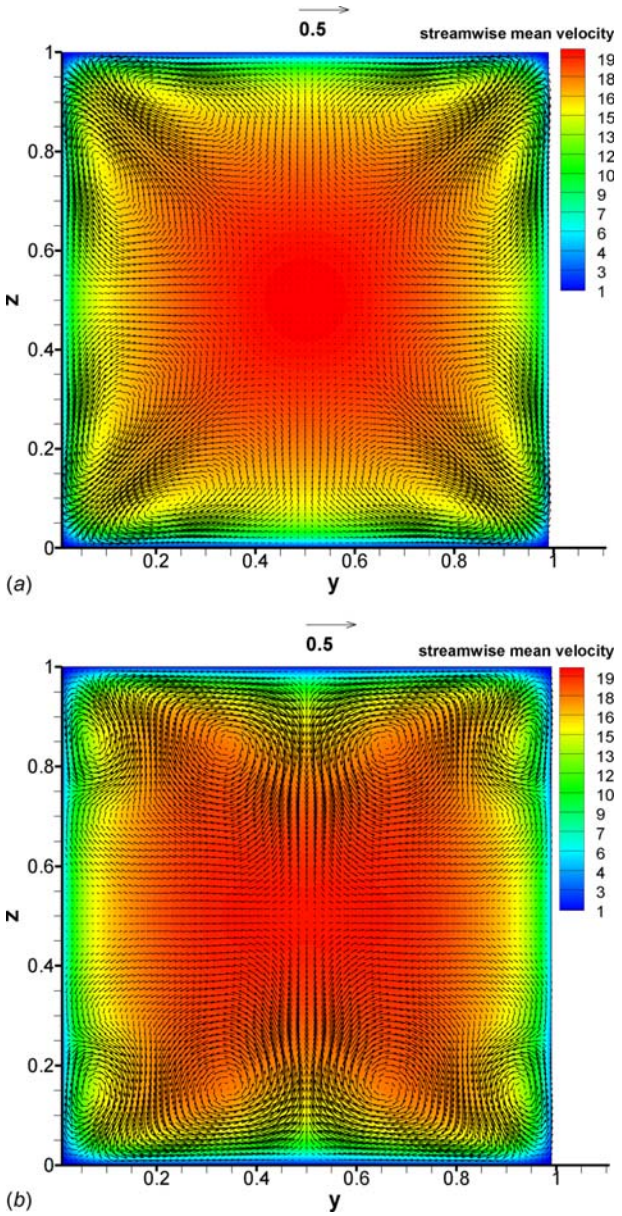


**Fig. 4 Time-averaged velocity field in a cross-sectional plane (*a*) non-MHD case and (*b*) MHD case**

**Particle Dispersion.** The deposition of particles on duct walls is directly a result of how the particles are transported by the turbulent eddies. The focus of this paper is to study the particle dynamics in turbulent duct flow with a magnetic field and to compare it with that in a non-MHD flow. The instantaneous flow is used to transport the particles injected at the duct inlet. Since only one-way coupling is considered in this study, the continuous phase flow velocities are not altered by particles.

It is well known from previous studies that particles preferentially concentrate in regions of low vorticity and high strain rate [9]. There are several ways to illustrate this effect. By overlapping the particle positions and the instantaneous velocity field, we can study how particles preferentially accumulate in certain regions versus others. It is also known that particles collect in regions of low swirling strength and high strain. Both of these can be attained from the fluid velocity gradient tensor used to identify vortices [22]. Since vorticity can arise from both swirl and shear, it is not a clearly defined quantity for particle accumulation. The swirl strength is also related to the magnitude of the centrifugal effect experienced by the particles. Another useful quantity to characterize the effects of flow structures on particle dispersion was proposed by Maxey [23] to be $\nabla \cdot \mathbf{u}_p$, which acts like a source term in the particle equation of motion. It is given by

$$\nabla \cdot \mathbf{u}_p \approx -\tau_p \nabla \mathbf{u}_f : \nabla \mathbf{u}_f \tag{17}$$

when only the drag force is included. Thus, positive double dot product of the fluid velocity gradient tensor gives rise to particle accumulation and negative double dot product shows particle voids. Small particle response times show less preferential concentration.

Winkler et al. [1,2] have previously studied particle accumulation by turbulence-driven secondary flows in a square duct without a magnetic field. However, their method recycled the particles from outlet to the inlet and also performed streamwise averaging of particle statistics. In the current study, particles are continuously injected with random locations at the inlet. Hence, the gradual preferential concentration of particles can be more clearly seen in our study.

Figure 5 shows the positions of particles at one instant in time for the MHD and non-MHD cases for two particle Stokes numbers. The cross-stream secondary velocities are also shown. It can be seen that the particles, as expected, accumulate in saddle regions of cross-stream vortices. The smaller particles (lower Stokes number) are less concentrated because of their faster adjustment to the flow, as also seen in Eq. (15). Figure 6 shows the contours of $\nabla \cdot \mathbf{u}_p$ obtained from the continuous flow field using the relation in Eq. (15). The particles will concentrate in regions of negative $\nabla \cdot \mathbf{u}_p$ and will be pushed out of positive $\nabla \cdot \mathbf{u}_p$ regions. The four instantaneous contours of $\nabla \cdot \mathbf{u}_p$ and the particle locations (dots) do indicate this correlation well. We notice that in most places the particles are concentrated where $\nabla \cdot \mathbf{u}_p$ is negative. There are essentially no particles in regions of positive $\nabla \cdot \mathbf{u}_p$ (red regions in color version). However, the correlation is not perfect because of the time varying $\nabla \cdot \mathbf{u}_p$ and the particle positions. Figures 7 and 8 show the preferential concentration of particles in planes parallel to the walls. Since the flow fields parallel to one set of walls are different from the other set, the particle distributions are also different. In both Figs. 7 and 8, it is seen that particles tend to accumulate in regions with low-velocity streaks. Comparison of the streamwise velocity streaks in Figs. 7(*a*) and 7(*b*) reveals a thinner and more elongated streaky structure in the MHD flow shown in Fig. 7(*b*) as reported previously in Ref. [17], which in turn lead to a more concentrated particle dispersion in the MHD flow for $St = 5$ particles. However, particles with a larger response time ($St = 15$) are more randomly distributed and not sensitive to this difference in the streak structures between the MHD and non-MHD case, as is observed in Figs. 8(*a*) and 8(*b*).

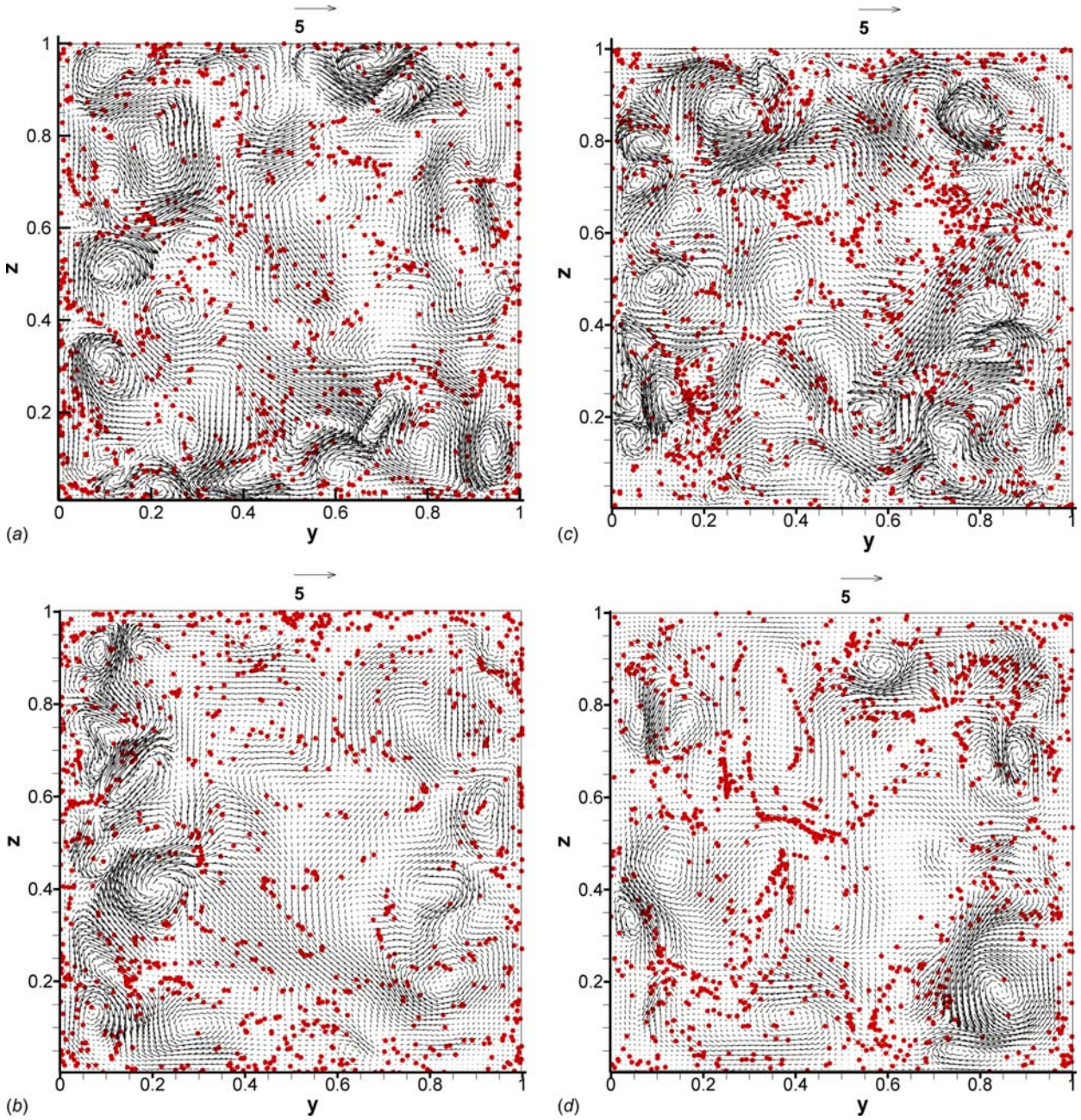


**Fig. 5 Instantaneous particle positions in a cross-sectional plane (*a*) non-MHD case, (St = 5), (*b*) MHD case, (St = 5), (*c*) non-MHD case, (St = 15), and (*d*) MHD case, (St = 15)**

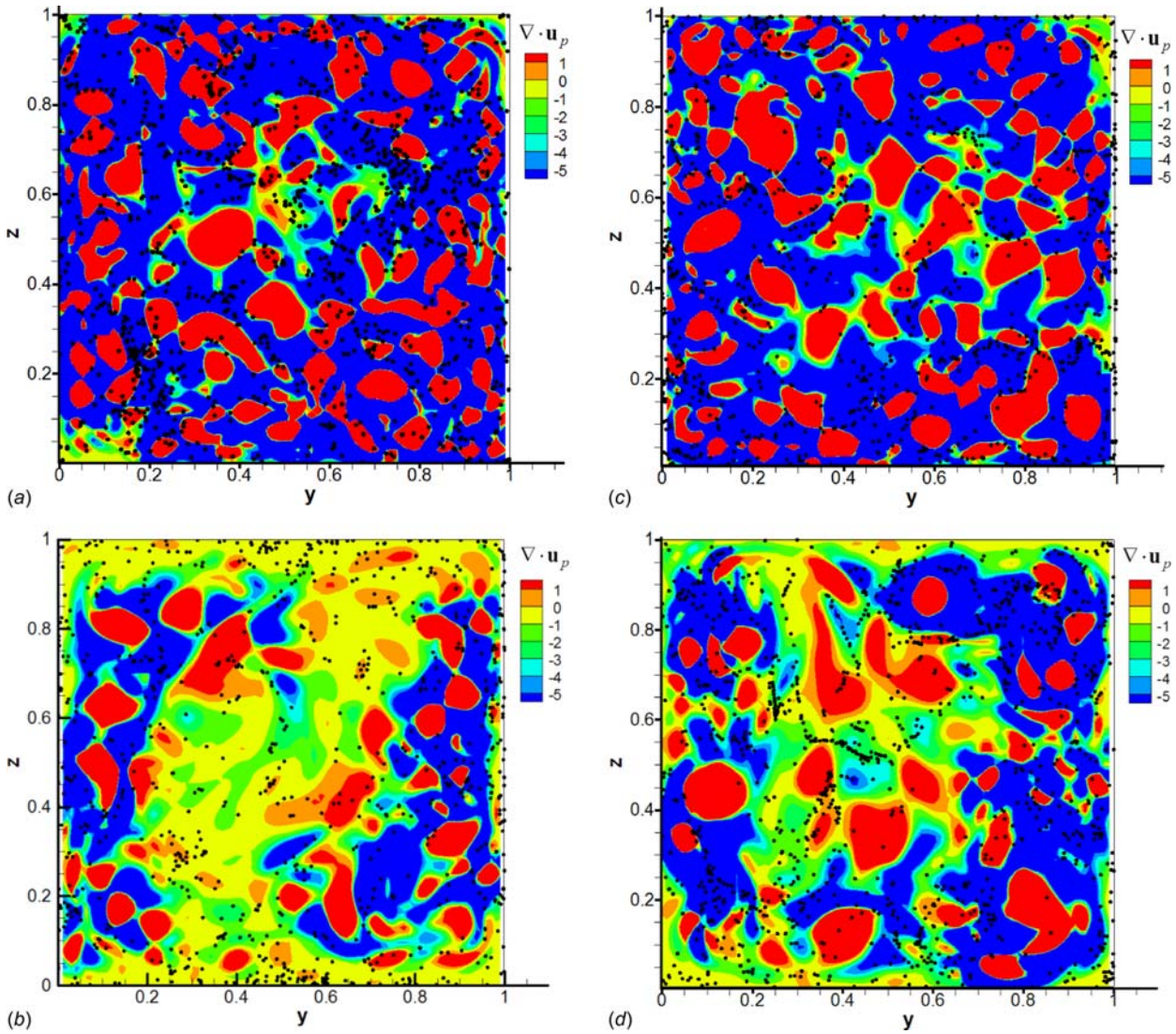


**Fig. 6 Preferential particle concentration in a cross-sectional plane (*a*) non-MHD case, St = 5, (*b*) MHD case, St = 5, (*c*) non-MHD case, St = 15, and (*d*) MHD case, St = 15**

### Particle Deposition

*Deposition Locations.* In this section, we present the particle deposition probability density distributions and particle preferential deposition locations. In order to numerically obtain a distribution of deposited particles in the streamwise direction, each duct wall is divided into 200 bins along the streamwise direction and the number of particles in each of the bins is counted, which is then divided by total number of particles to calculate the local deposition probability.

Total deposition of particles on duct walls is one of the key aspects of particle transport. Deposition of particles is influenced in a complex way by the local instantaneous flow velocities and the particle Stokes number as well as its instantaneous velocity from the previous time step. In the case of one-way coupling the continuous flow field is not modified by the particles; thus, the interaction is somewhat less complex. As the local flow fields with and without MHD are quite different, the deposition rates and patterns are quite different in the case of MHD and non-MHD duct flows. The probability distribution function of particle deposition along the streamwise direction is shown in Fig. 9 for the five particle Stokes numbers with and without MHD effects. An important observation from this study is that deposition probability of particles is decreased significantly by the imposed magnetic field for all the particle Stokes numbers. The deposition rate also decreases with the streamwise location along the square duct in all five cases. Initially, an increase of the slope close to the domain inlet is also observed. This might be a result of the random introduction of particles locations with local fluid velocity at domain entrance. This effect of initial condition vanishes after a small distance ($x = 0.5$) along the streamwise direction. The deposition probability increases significantly with particle Stokes number. As the Stokes number increases from 0.1 to 15, the probability distribution function (pdf) increases by approximately three orders of magnitudes for both MHD and non-MHD cases. As discussed by Brooke et al. [24], two different mechanisms are responsible for the particle deposition in wall-bounded turbulent flows: particle inertia and turbulent diffusion. For particles with higher inertia, they have the energy to penetrate the boundary layer and get deposited quickly, as described by the "free-flight" model [10, 20]. For low-inertia particles, the dominant way of deposition is through the turbulent diffusion. As particle Stokes number increases, the effect of particle inertia becomes more important in determining the deposition of particles.

The distribution of particle deposition pdf along the $y$- and $z$-directions on the duct walls are plotted in Figs. 10(*a*) and 10(*b*). These are summed over the length of the duct. Note that pdf distributions of particles deposited on opposite walls are expected to be

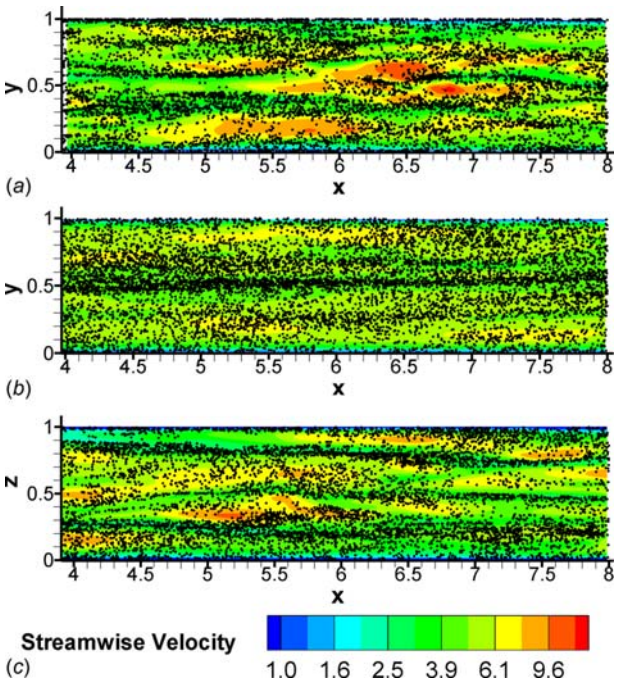


**Fig. 7 Instantaneous streamwise velocity contours with particle positions for St = 5 (*a*) non-MHD case, at $z^+ = 5$, (*b*) MHD case, at $z^+ = 5$, and (*c*) MHD case, at $y^+ = 5$**

statistically identical. Thus, the particle deposition pdfs presented in Fig. 10 are averaged over opposite walls. Figure 10(*a*) shows the particle deposition pdf on sidewalls parallel to the magnetic field ($y = 0$ and $y = 1$). It is observed that for all four cases, the deposited particles preferentially concentrate in regions close to the corner and in the central region of the wall. A wavy pattern for the preferential deposition locations is observed. For

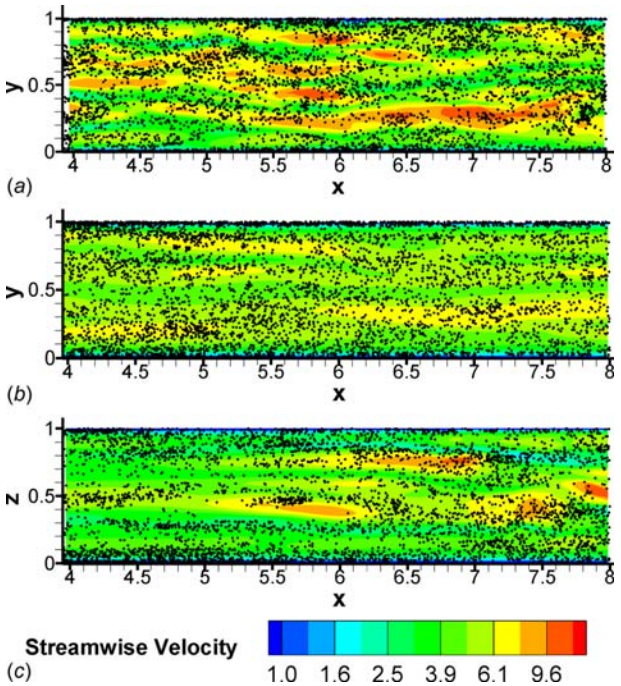


**Fig. 8 Instantaneous streamwise velocity contours with particle positions for St = 15 (*a*) non-MHD case, at $z^+ = 5$, (*b*) MHD case, at $z^+ = 5$, and (*c*) MHD case, at $y^+ = 5$**

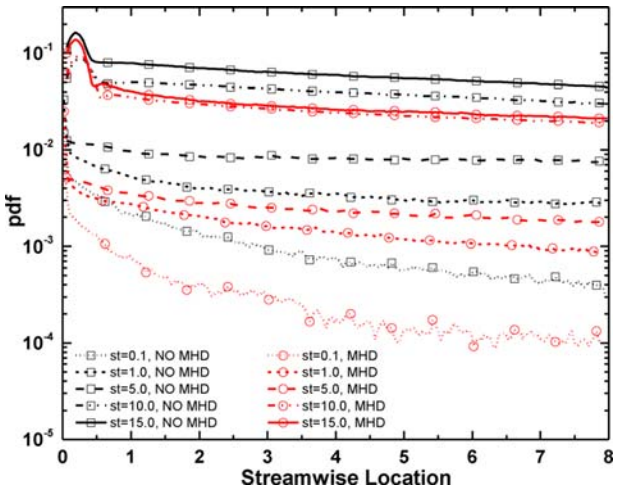


**Fig. 9 Probability distribution function of particle deposition location along streamwise direction**

the non-MHD case, particle deposition pdf patterns on sidewalls parallel and perpendicular to the magnetic field reflect each other, as expected. Higher particle response time (St = 15) tends to make the deposition patterns less preferential.

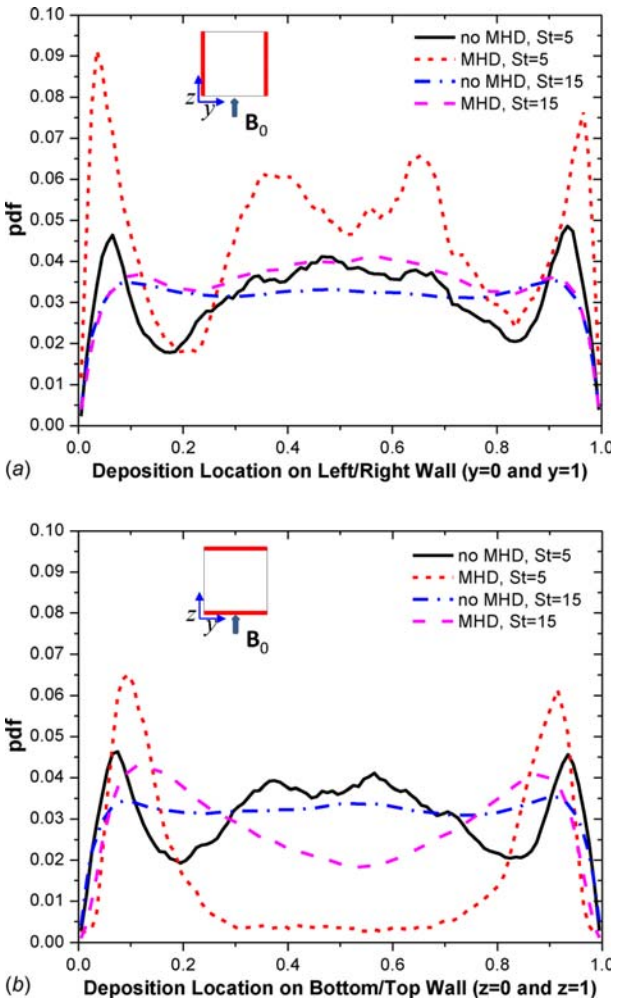


**Fig. 10 Probability distribution function of particle deposition location along spanwise and transverse directions (*a*) pdf on walls parallel to magnetic field and (*b*) pdf on walls perpendicular to magnetic field**

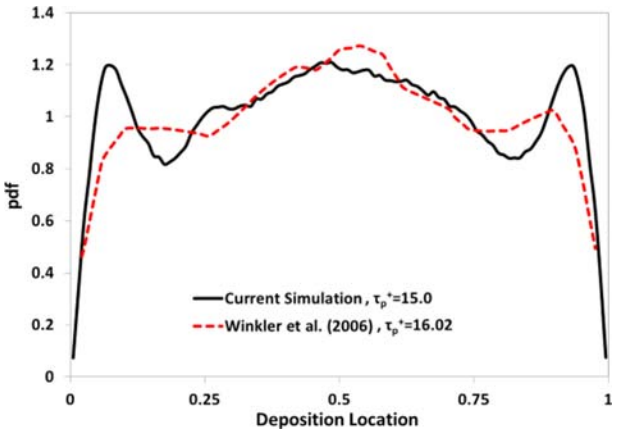


**Fig. 11 Comparison of particle deposition pdf for two particle releasing approaches**

In the MHD case (Fig. 10(*b*)), particles of smaller Stokes number (St = 5) have a higher variation in the pdfs on both parallel and perpendicular walls (to the magnetic field). Particles deposited on duct walls parallel to the magnetic field exhibit a more wavy distribution compared to the non-MHD case, while for walls perpendicular to the magnetic field, particle depositions show peaks near the two corners, with low particle deposition rate in the central region (between 0.2 and 0.8) of the walls. The particle deposition pdf in the central region is only 5% of that in the non-MHD case.

For the MHD case with a higher particle response time (St = 15), the pdf distributions between parallel (to magnetic field) and perpendicular walls have less variation compared to the cases with smaller particle response time. Particle distributions near duct corner regions are similar for parallel and perpendicular walls. However, the shape of the pdf curve in the central region has an inflection point. The total deposition rate on walls parallel to the magnetic field is higher than that on the perpendicular walls.

The effect of periodic cycling of particles versus random injection at inlet is examined in Fig. 11 by comparing particle deposition patterns of current simulation and calculation of Winkler et al. [2] for similar particle Stokes number. A reasonable match of particle deposition pdf in the middle region of the duct walls is seen between the two particle injection methods, with some difference at the corners. The current method of continuous random particle injection at the duct entrance leads to a local peak in the particle deposition near the duct corner, while the method with periodic particle cycling shows a relatively flat profile.

Figures 12(*a*) and 12(*b*) and Figs. 13(*a*) and 13(*b*) show the spatial distributions of particles deposited on the duct walls in both MHD and non-MHD cases for the lower particle response time (St = 5). These clearly show that the deposited particle distribution on parallel walls and perpendicular walls for non-MHD square duct flows are similar. However, for the MHD flow the particle deposition on walls perpendicular to the magnetic field are significantly different from the non-MHD flow case. It can be seen that in the presence of the magnetic field very few particles deposit in the central region of the wall. The particles on these walls deposit preferentially in regions close to the duct corners. Particle deposition on walls parallel to the magnetic field is seen to exhibit a streaky pattern in both MHD and non-MHD cases. The location of the deposited particles in Figs. 12(*a*) and 12(*b*) and Figs. 13(*a*) and 13(*b*) are an aggregate over a time span of $\Delta t^+ = 70$.

*Wall-Normal and Streamwise Deposition Velocities.* Particle deposition velocities are an important factor for pipe clogging and erosion. Figure 14 shows the wall-normal velocity distributions of the depositing particles with two different particle Stokes numbers

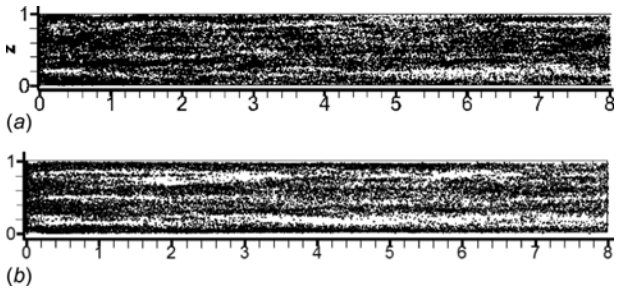


**Fig. 12 Particle deposition locations on walls parallel to the magnetic field (St = 5) (*a*) non-MHD case and (*b*) MHD case**

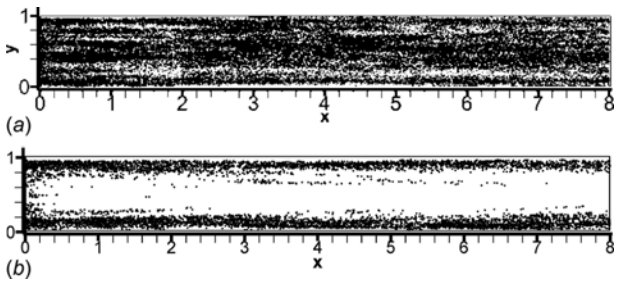


**Fig. 13 Particle deposition locations on walls perpendicular to the magnetic field (St = 5) (*a*) non-MHD case and (*b*) MHD case**

(St = 5 and 15) for both MHD and non-MHD cases. Wall-normal deposition velocities of the St = 5 and St = 15 particles are shown in Fig. 14(*a*), with wall-normal fluid velocities at $y^+ = 3.67$ plotted for comparison. It is seen that in the non-MHD case as shown in Fig. 14(*a*), the particle deposition velocities in the wall-normal direction for both Stokes numbers are higher than those of the continuous phase in the viscous sublayer ($y^+ = 3.67$). Also the wall-normal velocities of the deposited particles with larger response time (St = 15) on walls both parallel and perpendicular to the magnetic field (pointing towards positive $z$-axis) are about four times higher than those of the particles with the smaller response time (St = 5). It is also observed that for both particle Stokes numbers presented here (St = 5 and 15), a wavy profile of the particles wall-normal deposition velocities with valleys and peaks forms in the non-MHD case, which matches with previous results by Winkler [1]. The locations of the two secondary peaks for the particle wall-normal deposition velocities near the duct corners change slightly with the particle response time: larger particle response time (St = 15) tends to move the secondary peak locations toward the duct center (~13% of the duct width), while smaller particle response time (St = 5) keeps the secondary peak locations closer (~9% of the duct width) to the peak locations of the mean wall-normal velocities in the viscous sublayer (~5% of the duct width in the plane of $y^+ = 3.67$). Thus, it is suggested that for the non-MHD case from the comparison between the two particle Stokes numbers presented here (St = 5 and 15), wall-normal particle deposition velocities on walls both parallel and perpendicular to the magnetic field increase with particle response time by ~4 times (from St = 5 to St = 15). A wall-normal velocity peak exists around the duct center due to the lift force pointing toward the wall induced by a relatively large local streamwise velocity gradient, as reported previously by Winkler et al. [1].

Wall-normal velocity distributions of depositing particles in the MHD case on walls parallel and perpendicular to the magnetic field are presented in Figs. 14(*b*) and 14(*c*) for both particle response times (St = 5 and 15). It is clearly seen that wall-normal particle deposition velocities in the MHD case are significantly altered from those in the non-MHD case. The high wall-normal deposition velocity region at duct center in the non-MHD case has the lowest particle wall-normal deposition velocities, in the MHD

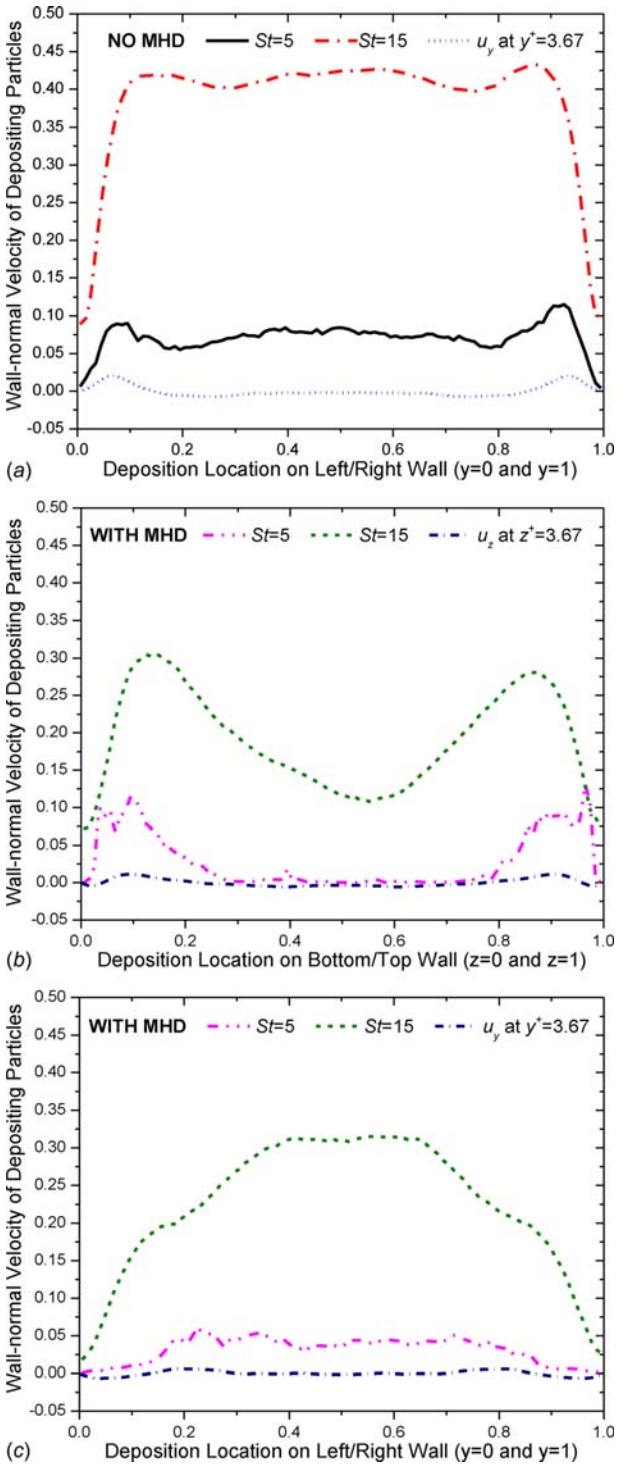


**Fig. 14 Wall-normal velocity distribution of depositing particles (*a*) non-MHD case, (*b*) MHD case, on walls perpendicular to magnetic field, and (*c*) MHD case, on walls parallel to magnetic field**

case on walls perpendicular to the magnetic field. The two secondary peaks in the wall-normal velocity profiles in the MHD case on walls perpendicular to the magnetic field stay at the same deposition locations as in the non-MHD case. However, the wall-normal particle deposition velocities at these secondary peaks on duct walls perpendicular to the magnetic field are ~30% less than those in the non-MHD case for particles with a higher response time (St = 15), and around the same for the smaller particle response time (St = 5). The wall-normal deposition velocities at duct center decrease by ~70% in the MHD case on walls perpendicular to the magnetic field for the larger particle response time (St = 15), and almost 100% for the smaller particle response time (St = 5). On walls parallel to the magnetic field, however, no secondary peaks for the particle wall-normal deposition velocities exist, leaving only the peak around duct center region, with the maximum averaged particle deposition velocity decreased by ~25% from that in the non-MHD case for St = 15 particles and ~50% for St = 5 particles.

Streamwise averaged depositing velocities for both St = 5 and St = 15 particles adopt similar peak locations with those for the wall-normal deposition velocities as seen in Figs. 15(*a*)–15(*c*). Mean fluid streamwise velocities at planes 3.67 wall units from the duct sidewalls are lower than the particle streamwise deposition velocities for St = 15 particles, but higher than those for the St = 5 particles in the non-MHD case, as shown in Fig. 15(*a*). In the MHD case on walls perpendicular to the magnetic field, particle deposition velocities are ~40% lower than the fluid mean velocities at duct center for St = 15 particles but more than one order of magnitude lower for St = 5 particles, as shown in Fig. 15(*b*). Figure 15(*c*) gives the streamwise mean profile of particle deposition velocities on walls parallel to the magnetic field, together with the fluid streamwise mean velocity profile in the viscous sublayer ($y^+ = 3.67$). The maximum streamwise deposition velocity on walls parallel to the magnetic field is decreased from ~5.6 in the non-MHD case to ~4.4 with a 21% reduction for St = 15 particles and a ~33% reduction for St = 5 particles.

*Deposition Rate*. Particle deposition rate has been defined in different ways in the literature [3,7,20]. In this work, the deposition rate is computed following Eq. (15), where $N_d$ is the number of particles deposited on all duct walls over a time span of $\Delta t_d$, $N_p$ is the number of particles in the domain with a volume $V$ and a deposition surface area $A$, and the deposition rate is nondimensionalized by the friction velocity $u_\tau$, as defined in Ref. [3]. However, it is worth pointing out that all definitions from Refs. [3,7,20] are equivalent to each other if only uniform-sized particles are considered.

$$V_d^+ = \frac{N_d V}{\Delta t_d N_p u_\tau A} \tag{18}$$

As shown in Fig. 16, current results of the total deposition rates in the non-MHD case agree well with the previous data from one-way coupling simulations of Winkler et al. [1,2], despite the difference in particle deposition pdf near duct corner region observed in Fig. 11. This agreement on deposition rate between previous work and current results suggests that the particle module in the current GPU code is implemented correctly and reinforces the pattern of particle deposition in a turbulent square duct flow, which is different than that in a pipe flow [11] and in annular flows [12].

It is observed that for larger particle Stokes numbers (e.g., St ≥ 5) in both MHD and non-MHD cases, the computed deposition rates match reasonably well with experimental correlations by both Liu [11] and McCoy [12]. Thus, deposition of particles of higher inertia is not influenced by the turbulence driven secondary flows compared with lower-inertia particles. For particles with lower inertia (e.g., St < 5), the deposition rates start to deviate from the experimental correlations for pipe flows and remain higher. This discrepancy is due to the effects of turbulence-induced secondary flows unique to noncircular ducts, which constantly send particles toward duct walls with a net effect of enhancing particle depositions.

In the MHD case, it is seen that the rate of particle deposition on walls parallel to the magnetic field is 2~5 times larger than that on walls perpendicular to the magnetic field. However, this difference reduces when the particle Stokes number increases (e.g., St > 5). It is seen that for St larger than 10, the particle

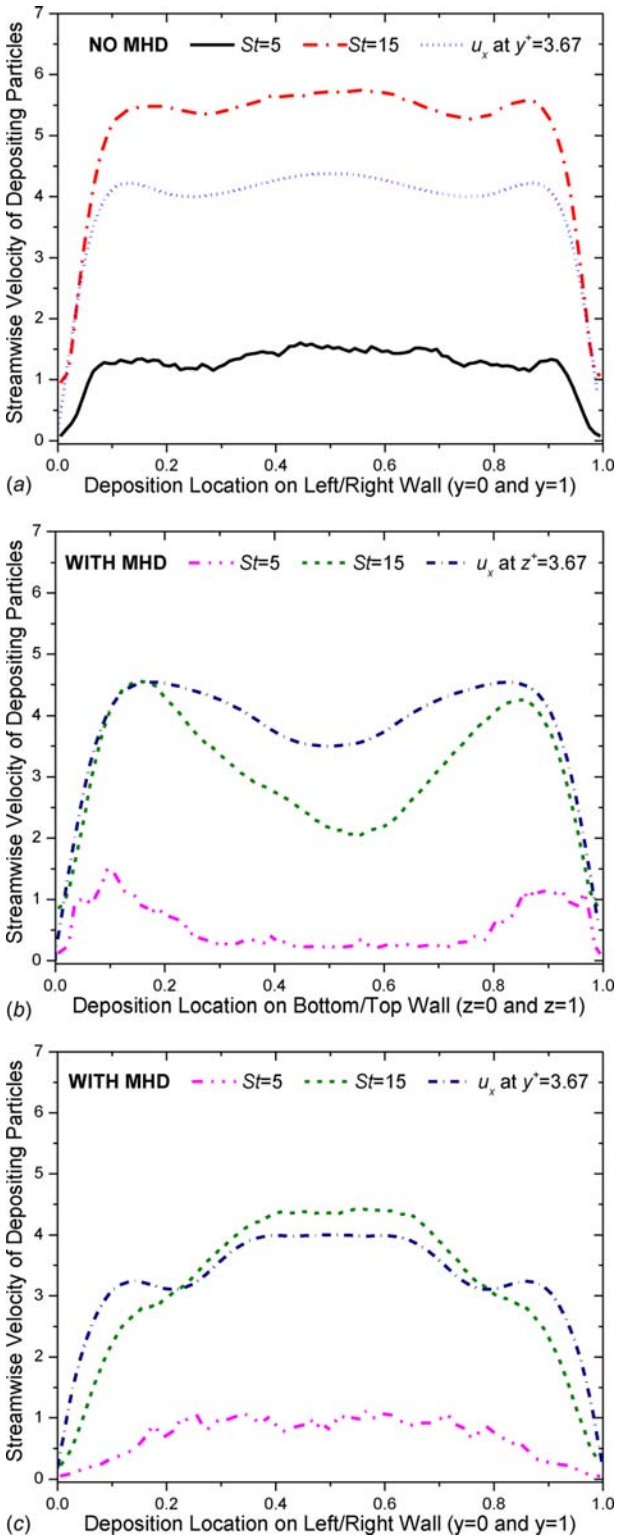


**Fig. 15 Streamwise velocity distribution of depositing particles (*a*) non-MHD case, (*b*) MHD case, on walls perpendicular to magnetic field, and (*c*) MHD case, on walls parallel to magnetic field**

deposition rate on walls parallel to the magnetic field is just slightly higher (~20%) than that on the walls perpendicular to the magnetic field. The deposition rates in the non-MHD case for all the particle Stokes numbers studied in current work are usually 2~5 times higher than those in the corresponding MHD

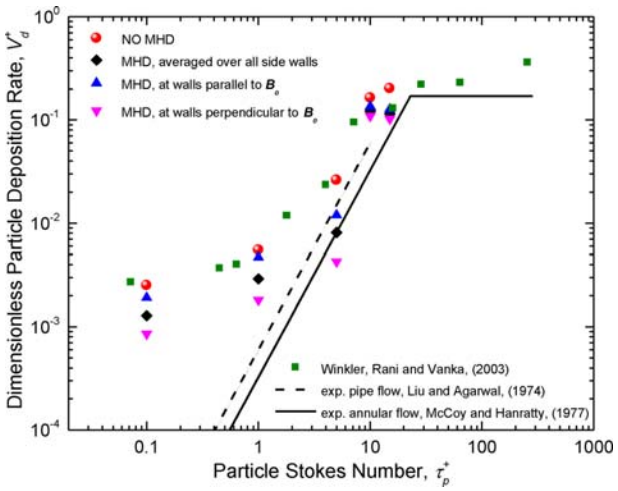


**Fig. 16 Dimensionless particle deposition rates**

case, while this ratio also decreases as particle response time increases.

## Conclusions

In this work, a DNS study on turbulent flow in a square duct with the effects of an imposed magnetic field was first performed, and then Lagrangian particle tracking was utilized to investigate particle dispersion and deposition using one-way coupling. Inclusion of a magnetic field modifies the flow in the streamwise direction as well as secondary mean flows. Turbulence is suppressed with the effect of an imposed magnetic field. Resultant secondary mean flow does not exhibit a symmetric pattern along the corner bisector any more, with the mean secondary eddies along the walls parallel to the magnetic field weakened and the one along the walls perpendicular to magnetic field shifted toward duct core.

In both MHD and non-MHD square duct flows, particles tend to accumulate in the saddle regions between turbulent eddies but away from the centers of the secondary vortices of the cross-flow direction. Along the streamwise direction close to the wall, particles tend to gather in regions with low velocity streaks. Pattern of particle deposition on the duct walls has been significantly altered by the imposed magnetic field, with the particle deposition rate decreased from ~7% to ~2% (e.g., for St = 5). Preferential particle deposition location for the non-MHD case is observed to have a wavy shape along the spanwise direction, with more particles deposited near the corner region, and in the central region of the wall. A similar deposition pattern is found in the MHD case at walls parallel to the direction of imposed magnetic field. However, at walls perpendicular to the magnetic field direction, the number of deposited particles decreases substantially in the central region, especially for particles with smaller Stokes number (e.g., St < 5), while more particles can be found near the corners of the duct. Increasing particle Stokes number increases particle deposition rate and particle deposition velocities in both the MHD and non-MHD cases. The average streamwise velocities of depositing particles are smaller than the local averaged fluid velocities at 3.67 wall units for smaller particles (e.g. St ≤ 5), but larger for larger particles.

Results from particle deposition rate calculations suggest that overall particle deposition rates in non-MHD cases are usually 2~5 times higher than those in the corresponding MHD cases, while this ratio drops to almost equal for particles with larger response times (e.g., St > 10), the deposition rates of which also follow the previous experimental correlations from pipe and annular flows. Deposition rates of particles with smaller response times in both MHD and non-MHD cases deviate from those correlations mainly due to the unique secondary flows induced by turbulence in square duct flows.

## Acknowledgment

This work is supported by Continuous Casting Consortium at University of Illinois, Urbana-Champaign, the National Science Foundation (Grant CMI 11-30882), and a NVIDIA Professor Partnership Grant. The assistance of Mr. Ramnik Singh and Dr. Rajneesh Chaudhary in providing the MHD version of CUFLOW is gratefully acknowledged.

## Nomenclature

$A$ = area of particle deposition
$\mathbf{B_0}$ = imposed magnetic field vector
$C_D$ = drag coefficient
$d_p$ = particle diameter
$\mathbf{F}_D$ = drag force
$\mathbf{F}_L$ = lift force
$\mathbf{J}$ = current
$L_{x,\,y,\,z}$ = Lagrange interpolation factor corresponding to $x$, $y$, $z$ in Cartesian system
$m_p$ = mass of a particle
$n$ = cell number
$N_d$ = number of deposited particle
$N_p$ = number of particles in the domain
$p$ = pressure
pdf = probability density function
$\mathrm{Re}_p$ = particle Reynolds number
$\mathrm{Re}_\tau$ = Reynolds number based on friction velocity
St = particle Stokes number
$t$ = time
$\mathbf{u}$ = fluid velocity vector
$u_\tau$ = friction velocity
$\nu$ = kinematic viscosity of fluid
$V$ = volume of the computational domain
$V_d^+$ = dimensionless particle deposition rate
$x, y, z$ = coordinates of the Cartesian system
$\Delta t_d$ = time span for particle deposition
$\rho$ = density (of fluid or particle)
$\mu$ = dynamic viscosity
$\phi$ = electric potential
$\sigma$ = magnetic conductivity
$\tau_p$ = particle response time
$\tau_p^+$ = dimensionless particle response time (St)
$\varphi$ = generic physical quantity

## Subscripts

$f$ = quantity related to fluid
$i, j, k$ = cell index corresponding to $x$, $y$, $z$ in the Cartesian system
$p$ = quantity related to particle

## References

[1] Winkler, C. M., Rani, S. L., and Vanka, S. P., 2004, "Preferential Concentration of Particles in a Fully Developed Turbulent Square Duct Flow," Int. J. Multiphase Flow, **30**(1), pp. 27–50.
[2] Winkler, C. M., Rani, S. L., and Vanka, S. P., 2006, "Numerical Study of Particle Wall-Deposition in a Turbulent Square Duct Flow," Powder Tech., **170**(1), pp. 12–25.
[3] Phares, D. J., and Sharma, G., 2006, "A DNS Study of Aerosol Deposition in a Turbulent Square Duct Flow," Aerosol Sci. Tech., **40**(11), pp. 1016–1024.
[4] Phares, D. J., and Sharma, G., 2006, "Turbulent Transport of Particles in a Straight Square Duct," Int. J. Multiphase Flow, **32**, pp. 823–837.
[5] Yao, J., and Fairweather, M., 2010, "Inertial Particle Resuspension in a Turbulent, Square Duct Flow," Phys. Fluids, **22**, p. 033303.
[6] Yao, J., and Fairweather, M., 2012, "Particle Deposition in Turbulent Duct Flows," Chem. Eng. Sci., **84**, pp. 781–800.
[7] Narayanan, C., and Lakehala, D., 2003, "Mechanisms of Particle Deposition in a Fully Developed Turbulent Open Channel Flow," Phys. Fluids, **15**(3), pp. 763–775.
[8] Elghobashi, S., 1994, ''On Predicting Particle-Laden Turbulent Flows," Appl. Sci. Res., **52**, pp. 309–329.
[9] Kulick, J., Fessler, J., and Eaton, J., 1994, "Particle Response and Turbulence Modification in Fully Developed Channel Flow," J. Fluid Mech., **277**, pp. 109–134.
[10] Friedlander, S. K., and Johnstone, H. F., 1957, "Deposition of Suspended Particles From Turbulent Gas Streams," Ind. Eng. Chem., **49**(7), pp. 1151–1156.
[11] Liu, Y. H., and Agarwal, J. K., 1974, "Experimental Observation of Aerosol Deposition in Turbulent Flow," Aerosol Sci., **5**, pp. 145–155.
[12] McCoy, D. D., and Hanratty, T. J., 1977, "Rate of Deposition of Droplets in Annular Two-Phase Flow," Int. J. Multiphase Flow, **3**, pp. 319–331.
[13] Germano, M., Piomelli, U., Moin, P., and Cabot, W. H., 1991, "A Dynamic Subgrid-Scale Eddy Viscosity Model," Phys. Fluids, **3**, pp. 1760–1765.
[14] Yuan, Q., Thomas, B. G., and Vanka, S. P., 2004, "Study of Transient Flow and Particle Transport During Continuous Casting of Steel Slabs, Part 1. Fluid Flow," Metallurg. Mater. Trans. B, **35**B(4), pp. 685–702.
[15] Yuan, Q., Thomas, B. G., and Vanka, S. P., 2004, "Study of Transient Flow and Particle Transport During Continuous Casting of Steel Slabs, Part 2. Particle Transport," Metallurg. Mater. Trans. B, **35**B(4), pp. 703–714.
[16] Chaudhary, R., Thomas, B. G., and Vanka, S. P., 2012, "Effect of Electromagnetic Ruler Braking (EMBr) on Transient Turbulent Flow in Continuous Slab Casting Using Large Eddy Simulations," Metallurg. Mater. Trans. B, **43**B (3), pp. 532–553.
[17] Chaudhary, R., Vanka, S. P., and Thomas, B. G., 2010, "Direct Numerical Simulations of Magnetic Field Effects on Turbulent Flow in a Square Duct," Phys. Fluids, **22**(7), p. 075102.
[18] Maxey, M. R., and Riley, J. K., 1983, ''Equation of Motion for a Small Rigid Sphere in a Nonuniform Flow," Phys. Fluids, **26**, pp. 883–889.
[19] Schiller, L., and Naumann, Z., 1935, "A Drag Coefficient Correlation," Z. Ver. Deutsch. Ing., **77**, pp. 318–320.
[20] Saffman, P. G., 1965, ''The Lift on a Small Sphere in a Slow Shear Flow," J. Fluid Mech., **22**, pp. 385–400.
[21] Shinn, A. F., Vanka, S. P., and Hwu, W. W., 2010, "Direct Numerical Simulation of Turbulent Flow in a Square Duct Using a Graphics Processing Unit GPU," 40th AIAA Fluid Dynamics Conference, Chicago, IL, June 28–July 1, AIAA Paper No. 2010-5029.
[22] Adrian, R. J., Christensen, K. T., and Liu, Z.-C., 2000, "Analysis and Interpretation of Instantaneous Turbulent Velocity Fields," Experiments Fluids, **29**, pp. 275–290.
[23] Maxey, M. R., 1987, "The Gravitational Settling of Aerosol Particles in Homogeneous Turbulence and Random Flow Fields," J. Fluid Mech., **174**, pp. 441–465.
[24] Brooke, J. W., Hanratty, T. J., and McLaughlin, J. B., 1994, "Free-Flight Mixing and Deposition of Aerosols," Phys. Fluids, **8**(10), pp. 3404–3415.